Electronic Supplementary Information (ESI) for

Hydrothermally prepared nanosized and mesoporous $Ce_{0.4}Zr_{0.6}O_2$ solid solutions with shape dependence of photocatalysis for degradation of methylene blue

Wei Tian,[a] Jun Yin,[b] Lingfei Wei, [a] Quanhao Shen, [a] Rehana Bibi, [a] Ming Liu, [a] Bin Yang, [a] Naixu Li, [a,*] and Jiancheng Zhou [a,c,d,*]

Experimental Section

Chemicals and Reagents

Cerium (III) Nitrate Hexahydrate ($Ce(NO_3)_3 \cdot 6H_2O$), Zirconyl (IV) chloride octahydrate ($ZrOCl_2 \cdot 8H_2O$), Sodium hydroxide (NaOH) and urea ($CO(NH_2)_2$) were purchased from Shanghai Chemical Reagent Company in analytical grade and utilized as received without further purification. Distilled water was used throughout the experiment process.

Material preparation

Nanorod and nanoparticle (RP)-shaped $Ce_{0.4}Zr_{0.6}O_2$ solid solution

$Ce_{0.4}Zr_{0.6}O_2$ RPs were fabricated with previously reported method with small modification.[1, 2] Typically, to a known aqueous NaOH (6M) was decanted a homogeneous aqueous $Ce(NO_3)_3 \cdot 6H_2O$ (0.02M) and $ZrOCl_2 \cdot 8H_2O$ (0.03M) under intensive agitation. Afterwards, the resulting mixture was stirred for 0.5 h and hydrothermally treated at 373K for 24 h. After cooling down to room temperature, the crude precipitate was collected via centrifugation, thoroughly rinsed with distilled water and alcohol several times, and dried in vacuo at 313K. Finally, the as-dried solid was well-ground and subjected to calcination at 823K for 4h with a ramp of 4.5K/min. Similarly, other $Ce_xZr_{1-x}O_2$ samples with different molar components (x=0, 0.2, 0.6, 0.8, 1.0) were obtained as references.

Nanosphere (SP)-like $Ce_{0.4}Zr_{0.6}O_2$ solid solution

$Ce_{0.4}Zr_{0.6}O_2$ SPs were accessed with Wang's method.[1, 2] Briefly, to an aqueous NaOH (6M) was decanted a homogeneous aqueous $Ce(NO_3)_3 \cdot 6H_2O$ (0.02M) and $ZrOCl_2 \cdot 8H_2O$ (0.03M) under intensive agitation. Then, the resulting mixture was stirred for 0.5 h and hydrothermally treated at 453K for 24 h. After cooling down to room temperature, the crude precipitate was collected via centrifugation, thoroughly rinsed with distilled water and alcohol several times, and dried in vacuo at 313K. Finally, the as-dried solid was well-ground and subjected to calcination at 823K for 4h with a ramp of 4.5K/min.

Nanopolyhedron(PH)-like $Ce_{0.4}Zr_{0.6}O_2$ solid solution

$Ce_xZr_{1-x}O_2$ solid solutions were synthesized via hydrothermal procedures similar

to the earlier reports.[3] Typically, to a known NaOH (0.1M) was decanted a homogeneous aqueous $Ce(NO_3)_3 \cdot 6H_2O$ (0.02M) and $ZrOCl_2 \cdot 8H_2O$ (0.03M) under intensive agitation. Afterwards, the resulting mixture was stirred for 0.5 h and hydrothermally treated at 453K for 24 h. After cooling down to room temperature, the crude precipitate was collected via centrifugation, thoroughly rinsed with distilled water and alcohol several times, and dried in vacuo at 313K. Finally, the as-dried solid was well-ground and subjected to calcination at 823K for 4h with a ramp of 4.5K/min.

Nanoegg(EG)-shaped $Ce_{0.4}Zr_{0.6}O_2$ solid solution

$Ce_xZr_{1-x}O_2$ EGs were synthesized via a hydrothermal route similar to the earlier report.[1, 2] Typically, to an aqueous urea (0.08 M) was decanted a homogeneous aqueous $Ce(NO_3)_3 \cdot 6H_2O$ (0.012M) and $ZrOCl_2 \cdot 8H_2O$ (0.018M) under intensive agitation. Afterwards, the resulting mixture was stirred for 0.5 h and hydrothermally treated at 393K for 8 h. After cooling down to room temperature, the crude precipitate was collected via centrifugation, thoroughly rinsed with distilled water and alcohol several times, and dried in vacuo at 313K. Finally, the as-dried solid was well-ground and subjected to calcination at 823K for 4h with a ramp of 4.5K/min.

NOTE: Shape, structure and lattice spacing of catalytic materials were summarized in Table S2.

Material characterization

X-ray diffraction (XRD) patterns were recorded on a Ultima IV multipurpose X-ray diffraction system with graphite-monochromated Cu Ka radiation (λ=1.54178 nm) under 40 kV and 30 mA in the diffraction angle range of 2θ=10-80° at a scanning rate of 10° min^{-1} and a step of 2θ=0.02°. Lattice spacing (d) was calculated from Bragg equation λ=2dsinθ or directly obtained from CasaXPS Software.

Raman spectra were collected in the Raman shift range of 100-800 cm^{-1} on a laser confocal micro-Raman spectrometer (Thermo Fisher Scientific DXR Raman Microscope) equipped with BX51 Research Microscope and 532 nm solid state laser as a excitation origin, which provides a respectively spectral and spatial resolution of 2 cm^{-1} and 1μm in the spectral range from 100 to 6000 cm^{-1}.

Textural properties of as-prepared samples were well explored by nitrogen adsorption-desorption at 77 K on a Micromeritics ASAP 2020M analyzer. All samples were degassed at 473 K for 8 h prior to the measurement. The specific surface area and pore size distribution were determined using the BET and the BJH methods, respectively.

Field emission scanning electron microscope (FESEM) images were obtained on a JEOL JSM-6700F field emission scanning electron microscopy (SEM) at 0.01kV to 30kV in high-vacuum mode. Morphology and size of as-prepared samples were carefully observed through transmission electron microscopy (TEM, JEM-3010) with an accelerating voltage of 100-300 kV. Ethanolic suspension of a given determinand

was submitted to ultrasonic crashing for ca. 5 min. A spot of the resulting highly dispersed mixture was dropped onto the carbon-coated copper grid to allow complete evaporation of ethanol for sample test.

Elemental mapping within a selected area was performed by an energy-dispersive X-ray spectrometer (EDS) attached to TEM FEI Tecnai F30. Chemical state and surface composition were carefully examined through X-ray photoelectron spectroscopy (XPS) AXIS Ultra DLD, Shimadzu/Kratos Analytical, Japan) with monochromatic Al Kαa radiation (1486.6 eV). All the binding energies were calibrated using the C1s peak at 284.8 eV.[4]

UV-Vis diffuse reflection spectroscopy (DRS) was measured in the wavelength region of 200-800 nm with a wavelength resolution of 0.1 nm and a step of 0.5 nm using $BaSO_4$ as a reference (100% reflectance) on a Shimadzu UV-2450 spectrophotometer equipped with a diffuse reflectance accessory.

Acid-base properties of the catalysts are illustrated by NH_3 and CO_2-TPD patterns collected on a Micromeritics AutoChem II 2920 automated chemisorption analyzer (Micromeritics Instrument (Shanghai)Ltd.) with a thermal conductivity detector (TCD). Prior to adsorption experiments, 0.1g of the catalyst sample were first degassed at 400 °C for 1 h under helium (He) atmosphere. Next, the sample was immersed in NH_3 or CO_2 flow at 100 °C for 0.5 h. Afterwards, the sample was rinsed with He for 1 h to exhaust physisorbed NH_3 or CO_2. TPD profiles were depicted by linearly heating the sample from 20 to 800 °C with a ramp of 10 °C·min^{-1} under He carrier gas. The desorbed gaseous components were monitored by a thermal conductor detector (TCD).

Photoelectrochemical experiments

The photoelectrodes were prepared by spreading aqueous slurries of various shaped $Ce_{0.4}Zr_{0.6}O_2$ materials over 0.49 cm^2 of indium tin oxide (ITO) glass substrate (≤7Ω/□) with adhesive tapes as spaces. The suspension was accessed by grinding a determinand (10 mg) with water (30 μL) and PEDOT/PSS ink (30 μL). Then the photoelectrodes were treated in air at 353K for 0.5h. The photoelectrochemical experiments were implemented in a standard three-electrode system in a quartz tank with a Pt wire as the counter electrode and Ag/AgCl (saturated aqueous KCl) as the reference electrode. The 150 W Xe lamp (Beijing NBeT Co., Ltd.) acted as a light source. The photoelectrodes were irradiated from the back (106 mW·cm^{-2}). The current difference between light and dark was denoted as net photocurrent.

Photocatalytic tests

Photocatalytic MB degradation over $Ce_xZr_{1-x}O_2$ under simulated sunlight was performed was conducted in a optical quartz reactor using 500W Xe lamp as a light source and cooling water as a heat eliminating medium for temperature control at ca.25^{o}C of the reaction system. Aqueous suspension of a catalyst (300 mg/250 ml) was subjected to vigorous agitation by a magnetic bar for 1h in dark. Next, the reaction last for 2h with light and stirring on. 5ml of suspension was extracted from the reactor every 0.5h and centrifuged to remove catalytic sample, leaving the

supernatant examined on a 752S ultraviolet and visible spectrophotometer to record absorbance (A) of MB aqueous solution (λ_{max} = 664 nm). The degradation rate (D) and apparent rate constant (k) as indexes of photocatalytic activity were estimated according to the following equations:

$$D = (1\text{-}A/A_e) \times 100\% \quad \text{(S1)}$$

$$kt = \ln(A_e/A) \quad \text{(S2)}$$

Where A_e and A respectively denote absorbance at MB sorption balance in dark instantaneous absorbance after a period of time t (min) under irradiation.

Table S1-S7

Table S1 D and k as a function of x in $Ce_xZr_{1-x}O_2$

x	D/%	$k \cdot 10^4 \cdot min^{-1}$
0	54.9	66.4
0.2	50.9	59.2
0.4	70.5	98.9
0.6	44.7	49.3
0.8	45.5	50.5
1	36.7	38.2

[a] hydrothermally fabricated as described in the section of material preparation

Table S2: Shape, structure and lattice spacing of catalytic materials

No.	Shape[a]	Structure[b]	lattice spacing (nm)		
			111[c]/011[d]	200[c]/002[d]	220[c]/112[d]
1	RP	cubic	0.308	0.267	0.189
2	EG	tetragonal	0.306	0.264	0.187
3	PH	tetragonal	0.300	0.258	0.184
4	SP	cubic	0.302	0.261	0.185

[a] RP=R+P=nanorod+nanoparticle**;** EG=nanoeggs; PH=nanopoly; SP=nanosphere

[b] determined by XRD and Raman results

[c] determined by XRD results and associated with cubic system

[d] determined by XRD results and associated with tetragonal crystal system

Table S3 Binding energies of O1s, Zr 3d and Ce 3d XPS spectra of $Ce_{0.4}Zr_{0.6}O_2$ samples with various shapes

Shape	O1s			Zr 3d		Ce 3d							
	A_3	A_2	A_1	A_2	A_1	B	B_1	B_2	B_3	A	A_1	A_2	A_3
RP	529.4	531.6	533.2	181.7	184.1	882.3	885.1	888.8	898.1	900.6	903.3	907.5	916.6
PH	529.9	531.9	533.4	182.1	184.5	882.6	885.7	889.3	898.5	901.2	904.2	908.2	917.0
EG	529.6	531.3	532.8	182.0	184.4	882.6	885.9	889.3	898.3	901.0	904.2	907.8	916.7
SP	529.6	531.5	533.1	181.9	184.3	882.4	885.3	889.3	898.2	900.7	902.6	907.6	916.6

Table S4 XPS[a] and EDS quantitively analytical data of various morphological samples

Shape	Theoretical component	Surface real component		Ce^{3+} content	O species content in O1s spectra		
		XPS result	EDS result		A_1	A_2	A_3
RP	$Ce_{0.4}Zr_{0.6}O_2$	$Ce_{0.39}Zr_{0.61}O_2$	$Ce_{0.46}Zr_{0.54}O_2$	14.8%	20.5%	35.8%	43.7%
PH		$Ce_{0.50}Zr_{0.50}O_2$	$Ce_{0.48}Zr_{0.52}O_2$	20.5%	24.9%	33.4%	41.7%
EG		$Ce_{0.53}Zr_{0.47}O_2$	$Ce_{0.47}Zr_{0.53}O_2$	14.9%	14.8%	25.1%	60.0%
SP		$Ce_{0.50}Zr_{0.50}O_2$	$Ce_{0.49}Zr_{0.51}O_2$	17.8%	12.0%	20.8%	67.1%

[a] All data are peak area-based calculations.

Table S5 Textural property and adsorbance capacity of samples

Sample morphology	Textural property			MBA[d]
	S_{BET}[a]	PV[b]	APS[c]	
RP	39.6	0.150	15.1	29.6
SP	63.0	0.237	15.0	41.1
PH	47.0	0.164	14.0	1.56
EG	54.7	0.0742	5.43	15.1

[a] S_{BET} = BET surface area, $m^2 \cdot g^{-1}$

[b] PV = pore volume, $cm^3 \cdot g^{-1}$

[c] APS= average pore size, nm

[d] MBA= methylene blue adsorbance, %; MBA=1-A_e/A_o, where A_e and A_o represent absorbances of aqueous methylene blue at the adsorption-desorption balance in dark and its original solution.

Table S6 Controlled experiments

Title	Sample	light source	*D*/% [a]
1	RPs	Xe lamp	70.5
2	none	Xe lamp	43.1
3	RPs	none	0
4	none	none	0
5	TS-1	Xe lamp	0
6	1wt%-Ce/TiO_2	Xe lamp	90.3
7	WO_3	Xe lamp	43.0
8	$BiVO_4$	Xe lamp	98.2
9	g-C_3N_4	Xe lamp	46.6 [b]
10	g-C_3N_4/WO_3	Xe lamp	87.9 [c]

[a] authors' results in this paper

[b] the reference result[5]

[c] the reference result[6]

Controlled experiments are of great significance for further knowledge of RPs. In Table S6, MB discolouration over RP-shaped material turns out to be a typical light-driven catalytic process instead of a thermocatalytic or self-degradation one on the basis of blank tests (Title 1-4). Compared with those of reference samples (D = 90.3~98.2%,Title 6,8-10), the photocatalytic performance of RPs is very modest and there is still huge room for improvement such as via construction of RPs-based heterostructure like Title 10.

Table S7 Important data from the reactive species trapping experiments over RPs

Title	Free radical	Scavenger	D/%
1	blank	none	70.5
2	$\cdot O_2^-$	benzoquinone (0.1mM)	67.4
3	OH·	isopropanol (0.01M)	42.5
4	h^+	EDTA-2Na (2mM)	37.8

Precisely recognized reactive species are crucial for reaction mechanism proposal. In Table S7, remarkably diminished D values upon addition of isopropanol and EDTA-2Na (Title 1, 3-4) indicate OH· and h^+ as major active species. Equally, $\cdot O_2^-$ is well-defined as a minor one. Notably, h^+ as one of major active species further implies MB degradation is a first-order kinetic process (Fig.6b) mainly affected by MB adsorption.

Figure S1-S9

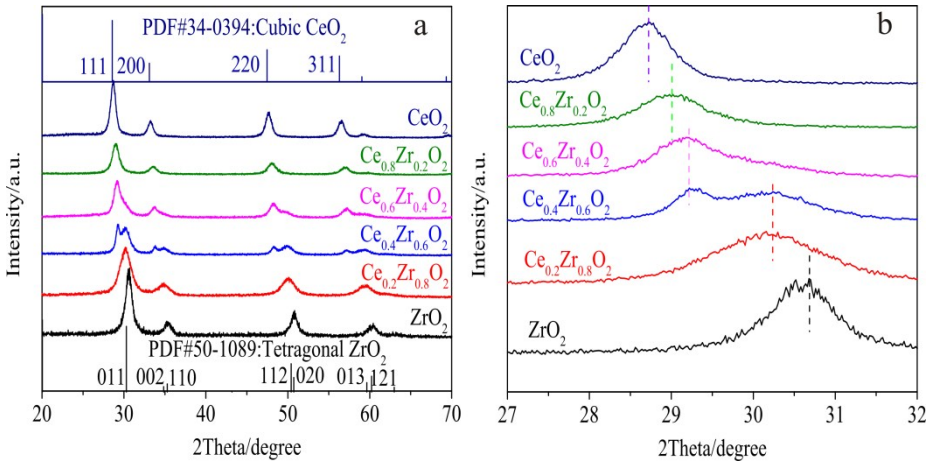

Fig.S1 (a) pristine and (b) locally magnified XRD patterns of $Ce_xZr_{1-x}O_2$ solid solutions with various components after alkaline hydrothermal treatment with 6M NaOH solution at 373K for 24h.

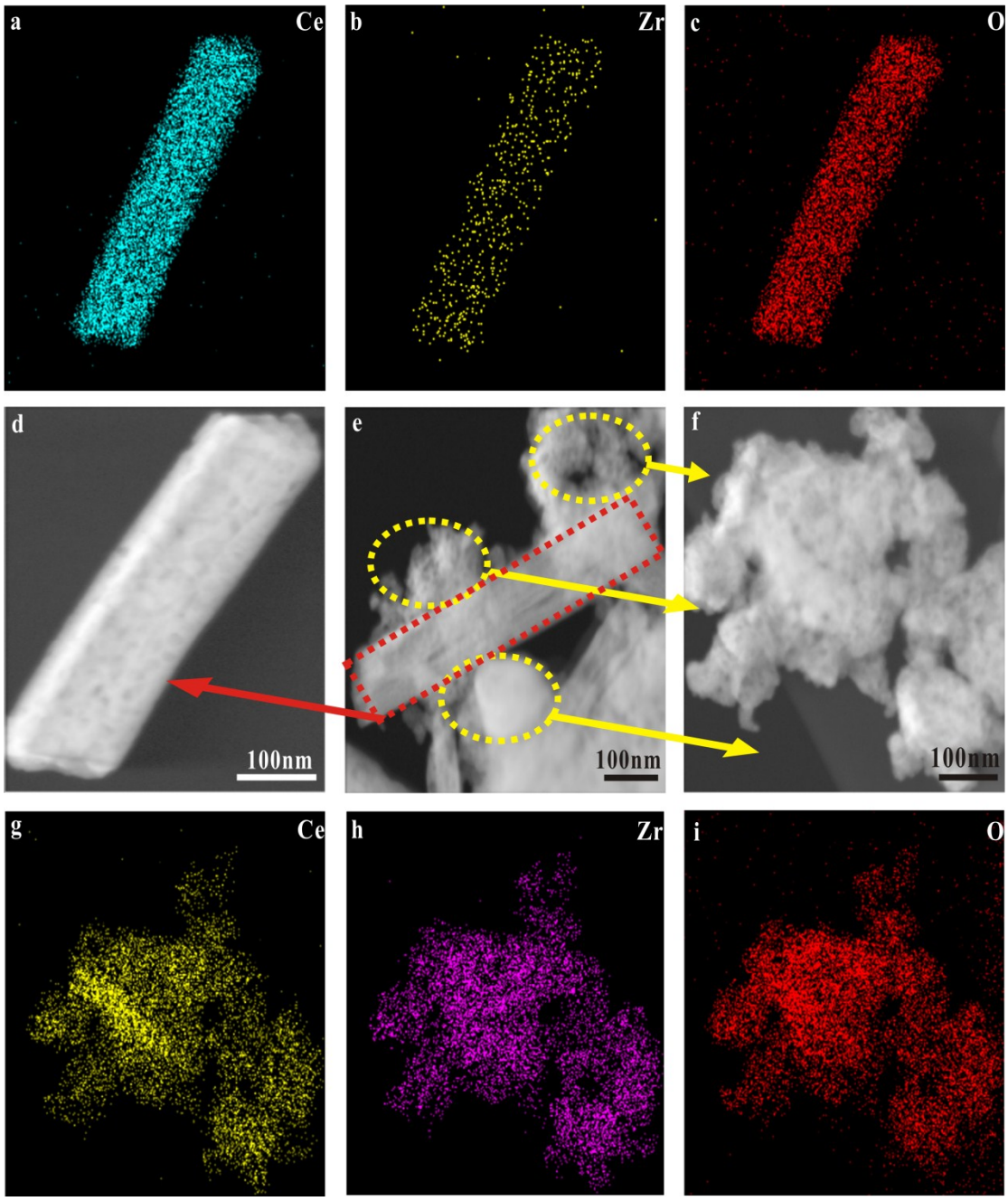

Fig.S2 STEM of RP -shaped $Ce_{0.4}Zr_{0.6}O_2$ (e) consisting of STEM and Ce, Zr and O mapping of R-shaped $Ce_{0.59}Zr_{0.41}O_2$ (a-d) and P-shaped $Ce_{0.21}Zr_{0.79}O_2$ (f-i).

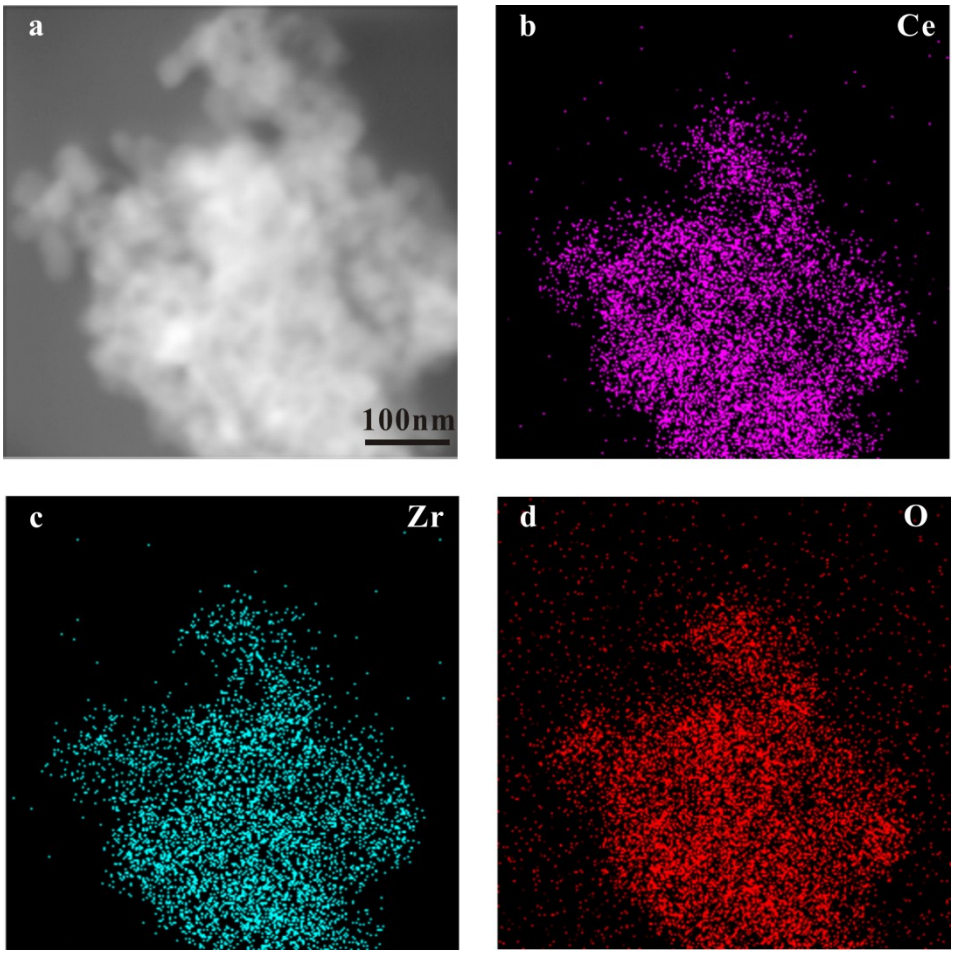

Fig.S3 STEM (a) and Ce, Zr and O mapping (b-d) of $Ce_{0.4}Zr_{0.6}O_2$ PHs

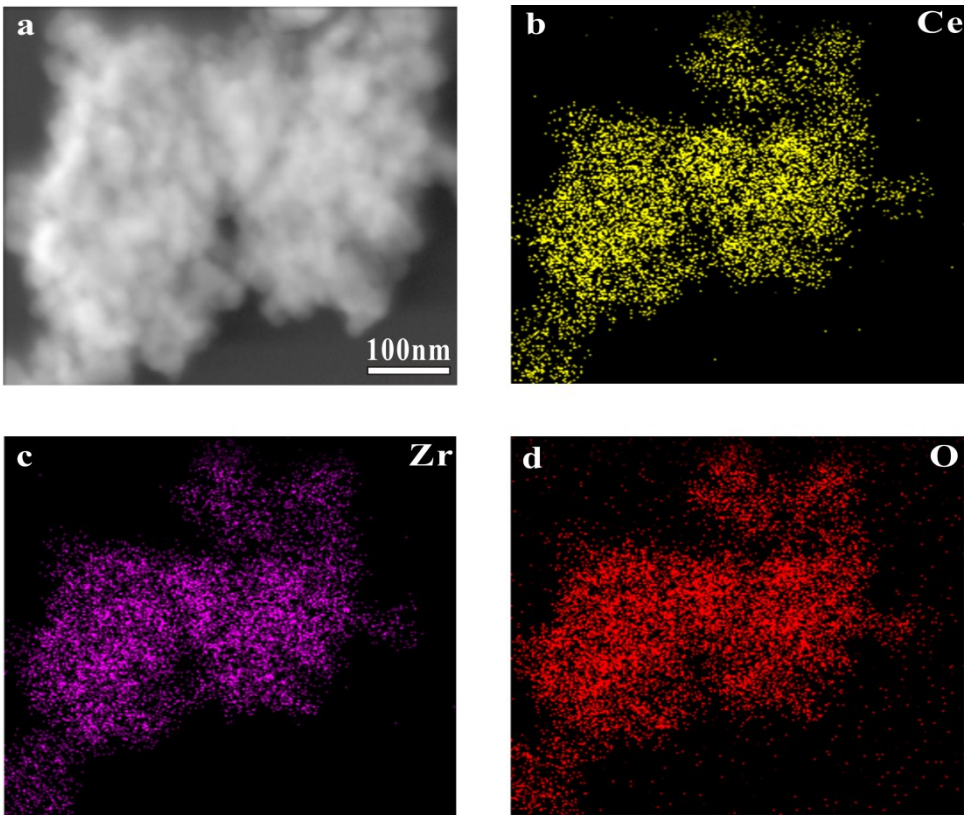

Fig.S4 STEM (a) and Ce, Zr and O mapping (b-d) of $Ce_{0.4}Zr_{0.6}O_2$ SPs

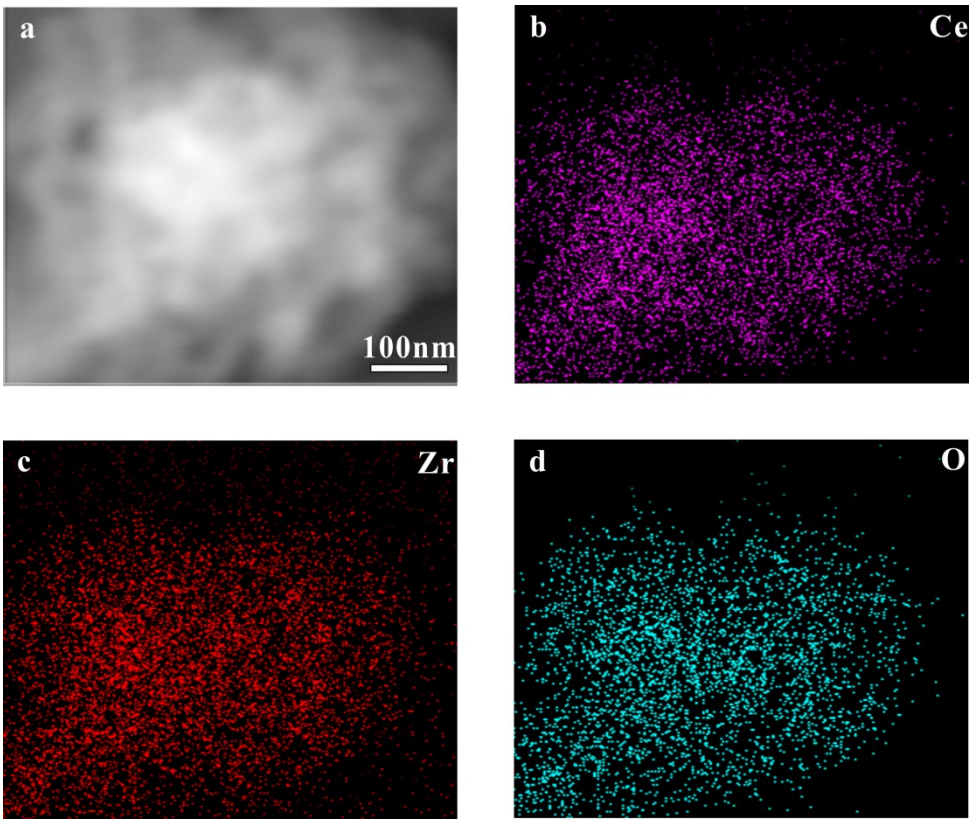

Fig.S5 STEM (a) and Ce, Zr and O mapping (b-d) of $Ce_{0.4}Zr_{0.6}O_2$ EGs

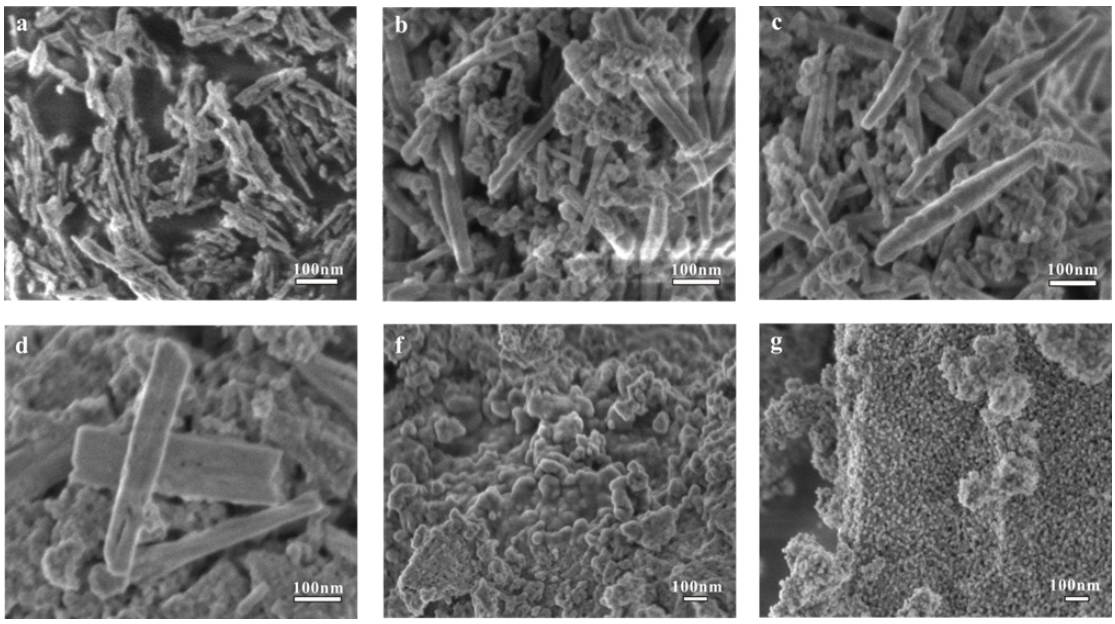

Fig.S6 SEM imagines of hydrothermally prepared $Ce_xZr_{1-x}O_2$ ($0 \leq x \leq 1$) with a NaOH concentration of 6 M at 373K for 24h； Graph sequence: a→g ~ CeO_2→ZrO_2.

SEM images in Fig.S6 gives shape to Zr loading-dependent shapes of samples

fabricated via a hydrothermal route with a 6 M NaOH at 373K for 24h (Table S2, No.1-6). Under such condition, enhanced Zr loading leads to gradually morphological transfer from CeO_2 Rs to ZrO_2 Ps. Thus, there is no surprising that intermediate constiuents such as $Ce_{0.4}Zr_{0.6}O_2$ feature as shape splitting towards R and P.

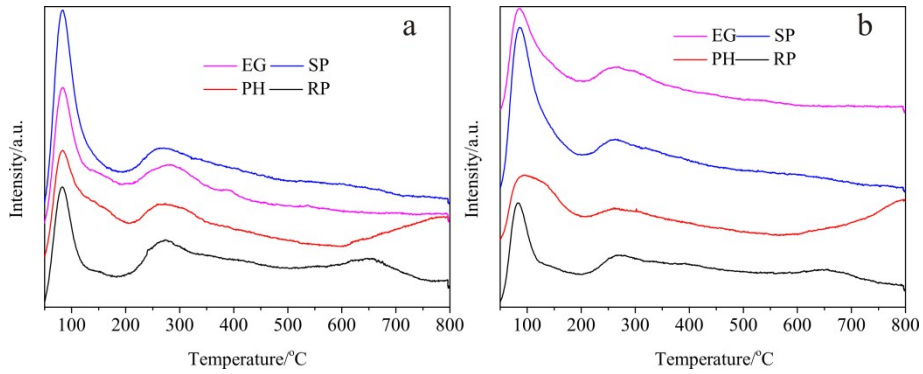

Fig.S7 NH_3 (a) and CO_2 (b) TPD curved lines of the samples with different morphologies.

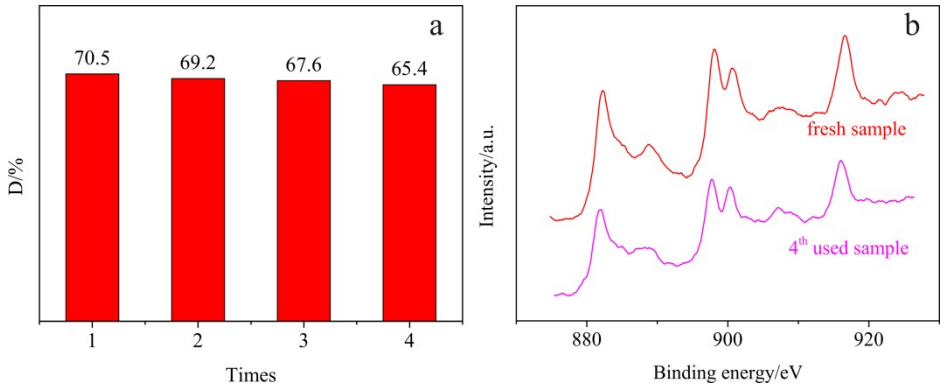

Fig.S8 (a) Reuse of RP-shaped $Ce_{0.4}Zr_{0.6}O_2$ and (b) Ce 3d XPS patterns of the fresh and 4th-used RP-shaped $Ce_{0.4}Zr_{0.6}O_2$.

A chemically and structurally stable catalytic material is in powerful demand for its catalytic application. RP-shaped body deserves this title by virtue of its activity and structural maintainance (Fig.S8a and8b) after 4th use.

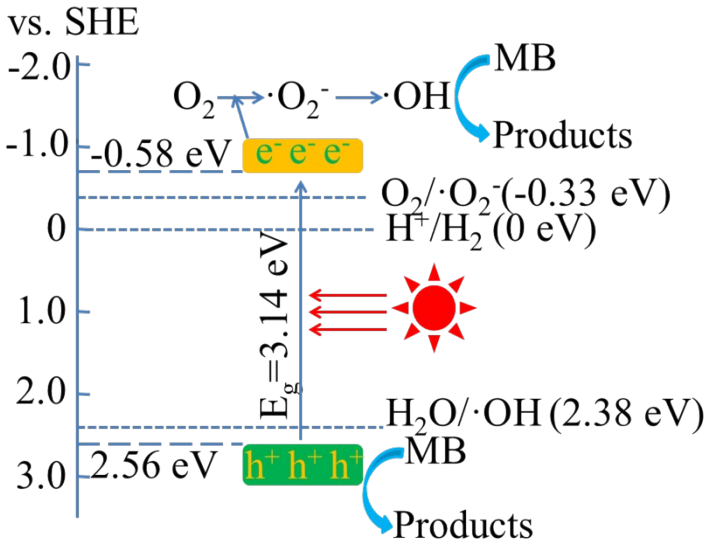

Fig.S9 Possible photocatalytic mechanism of MB over $Ce_{0.4}Zr_{0.6}O_2$ RPs

Table S7 provides solid evidence that ·OH and h^+ are major active species. Besides, Fig.4 indicates that RPs corresponds to a uniphase semiconductor with a given band structure (E_g =3.14eV, E_{CB}= -0.58 eV and E_{VB}=2.56 eV). Based on these facts, a possible mechanism for MB degradation over RPs is proposed.

Photogenerated e^--h^+ pairs are obtained upon the exposure of Xe lamp and enriched on CB and VB of the semiconductor, respectively. In most cases, e^- species are subsequently captured by dissolved O_2 to yield reactive oxygen species (ROS) such as $\cdot O_2^-$, $HO_2\cdot$ and ·OH.[7] Among them, the birth of $\cdot O_2^-$ is driven by the most negative potential (-0.33eV). In light of more negative E_{CB} (-0.58 eV) than that of $O_2/\cdot O_2^-$, it is not difficult to conclude that E_{CB} is more negative than potentials that drive formation of ROS including ·OH. Therefore, O_2 combines with e^- to obtain ·OH at last to degrade MB after several transformations. However, despite more positive E_{VB} (2.56 eV) than the potential of H_2O /·OH (2.38 V), h^+ does not oxidize H_2O to form ·OH but directly discolors MB possibly due to MB degradation as a first-order kinetic process mainly affected by MB adsorption (Fig.6b).

Reference

1. S. P. Wang, L. F. Zhao, W. Wang, Y. J. Zhao, G. L. Zhang, X. B. Ma and J. L. Gong, *Nanoscale*, 2013, **5**, 5582-5588.
2. H.-X. Mai, L.-D. Sun, Y.-W. Zhang, R. Si, W. Feng, H.-P. Zhang, H.-C. Liu and C.-H. Yan, *J. Phys. Chem. B*, 2005, **109**, 24380-24385.
3. R. Si and M. Flytzani-Stephanopoulos, *Angew. Chem.*, 2008, **120**, 2926-2929.
4. M. Liu, K. D. Gilroy, H.-C. Peng, M. Chi, L. Guo and Y. Xia, *Chem. Commun*, 2016, **52**, 13159-13162.
5. J. H. Liu, T. K. Zhang, Z. C. Wang, G. Dawson and W. Chen, *J. Mater. Chem.*, 2011, **21**, 14398-14401.
6. S. F. Chen, Y. F. Hu, S. G. Meng and X. L. Fu, *Appl. Catal., B*, 2014, **150**, 564-573.
7. L. Gu, J. Wang, Z. Zou and X. Han, *J. Hazard. Mater.*, 2014, **268**, 216-223.